



# Model of compact star with ordinary and dark matter

P. Mafa Takisa<sup>1</sup> · L.L. Leeuw<sup>2</sup> · S.D. Maharaj<sup>3</sup> 

Received: 8 July 2020 / Accepted: 3 October 2020 / Published online: 12 October 2020  
© Springer Nature B.V. 2020

**Abstract** We study compact stars formed by dark and ordinary matter, with attributes of both neutron star matter and quark star matter. We assume an equation of state for dark matter which is consistent with the rotational curves of galaxies and for color-flavor-locked (CFL) distributions for ordinary matter. This is done in the curved Krori-Barua spacetime geometry in general relativity. We find new exact solutions of dark matter admixed compact objects, with maximum mass  $2.67 M_{\odot}$  and radius around 11.16 km, with 52.40% of dark matter content. By varying the dark matter ratio, we obtain the masses of dark compact stars with masses less than  $2.67 M_{\odot}$ .

**Keywords** Einstein equations · Compact stars · Equation of state

## 1 Introduction

A quark star is made up of self-bound strange quark matter and its also known as a hypothetical stellar object (see

Witten (1984), Itoh (1970), Farhi and Jaffe (1984), Weber (2005), Ivanenko and Kurdgelaidze (1965) and Mukhopadhyay and Schaffner-Bielich (2016)). The equation of state for quark stars is not well understood which leads to controversies. The most known equation of state for compact stars composed of quark matter is the MIT bag model (Chodos et al. (1974)). Since Witten's work on quark matter (Witten (1984)) many investigations have been conducted in order to describe realistic physical features of these stellar compact objects. For more details see Haensel et al. (1986), Alcock et al. (1986), Benvenuto and Horvath (1989), Lugones and Horvath (2002, 2003), Alford et al. (2005), Bodmer (1971), Terazawa et al. (1978) and Rocha et al. (2019). The discovery of new observed pulsars with mass above  $1.97 M_{\odot}$  challenges the theoretical approach in describing compact stars. Some studies have suggested that these compact stars might be made up of stable dark matter with non-annihilating particles. The underlying assumption is that dark matter particles can accumulate inside the stellar core of the object (Ciarcelluti and Sandin (2011)).

From observations at galactic scales, the proof of dark matter presence with a large fraction of matter in our universe is an inevitable fact. Based on the above mentioned statement, it is believed that some dark matter could accumulate inside the stellar structure. This process could take place at the stellar birth and during a star's lifetime (Sandin and Ciarcelluti (2009)). For this purpose, in the past few years, attention has been given to study dark matter in relation to compact stars (quark stars, neutron stars and white dwarf stars). The hypothesis is that compact stars due to their high particle density should easily capture dark matter. Therefore compact objects may be likely candidates to help in constraining dark matter models (see Ade et al. (2016), Arcadi et al. (2012) and Feng (2012)).

✉ S.D. Maharaj  
maharaj@ukzn.ac.za

P. Mafa Takisa  
pmafatakisa@gmail.com

L.L. Leeuw  
lleeuw@uwc.ac.za

<sup>1</sup> Science, Engineering and Technology, School of Physics, University of South Africa, Florida Science Campus, P O Box 392, Unisa 0003, South Africa

<sup>2</sup> Department of Physics and Astronomy, University of the Western Cape, Bellville 7535, South Africa

<sup>3</sup> Astrophysics Research Centre, School of Mathematics, Statistics and Computer Science, University of KwaZulu-Natal, Private Bag X54001, Durban 4000, South Africa

In recent years more attention has been given to the study of the effect of dark matter effect on compact objects. The physical properties of compact objects can be changed by the presence of self-annihilation of dark matter in their core region (Angeles et al. (2012)). Several investigations have been conducted in recent years on dark matter admixture compact stars. The approach is based on two-fluid systems composed of dark matter and ordinary matter interacting basically through gravity (see Li et al. (2012), Sandin and Ciarcelluti (2009), Leung et al. (2011) and Kouvaris and Tinyakov (2010)). The first numerical solutions of dark matter in an admixed neutron star using the equation from curves of galaxies were found by Rezaei (2017, 2018). In their paper Mukhopadhyay and Schaffner-Bielich (2016) studied the quark stars admixed with dark matter. Despite all the mentioned studies, exact models of compact stars with an equation of state for dark matter are scarce. As yet there is no exact model of stellar objects with an equation of state for dark matter from the rotational curves of galaxies. Therefore it is worthwhile to study analytically the effect of dark matter on compact stars with this type of equation of state. Due to the complexity in solving the Einstein field equations in an exact approach, we solve the field equations with each equation of state separately, and apply the two fluid model of dark matter admixed ordinary matter through gravity interactions.

The paper is structured as follows. In Sect. 2 we present the Einstein field equations. New exact anisotropic solutions is generated in Sect. 3. In Sect. 4 the physical requirements for acceptability of the stellar model and the model parameter constraints are displayed. We present the two fluid formalism in Sect. 5. We display in Sect. 6 the results of masses and radii for the model. Physical features are presented in two tables, and also graphical plots of the matter variables for stellar structures are given. A detailed analysis of the physical features is given. A summary is made in Sect. 7.

## 2 The model

We choose the following metric for a static spherically interior matter distribution

$$ds^2 = -e^{\nu(r)} dt^2 + e^{\lambda(r)} dr^2 + r^2(d\theta^2 + \sin^2\theta d\phi^2), \quad (1)$$

where the gravitational potentials  $\nu(r) = Ar^2$  and  $\lambda(r) = Br^2 + C$ , with  $A$ ,  $B$  and  $C$  as constants. This form of the metric arises in the model of Krori and Barua (1975) which leads to a charged isotropic fluid sphere which is well behaved and singularity free. The simple form of the gravitational potentials leads to tractable expressions for the matter variables which allow for a physical analysis. The introduction of anisotropy is possible and allows for the description of several types of astrophysical objects. This approach

has been followed by several authors. For example Rahaman et al. (2012) obtained a strange star solution in general relativity and Sharif and Saba (2018) found a stellar model in an extended theory of gravity with anisotropy. We choose the above form of the metric with anisotropic pressures in our investigation; the equation of state is selected so that known cases are regained as special cases.

In our work we are using geometrized units where  $G = c = 1$ , which implies that the energy density is equal to mass density. For anisotropic distributions, the matter tensor can be written as follows

$$T_{ab} = \text{diag}(-\rho, p_r, p_t, p_t), \quad (2)$$

where  $\rho$ ,  $p_r$  and  $p_t$  are the total energy density, total radial pressure and total tangential pressure. The total anisotropy is given by  $\Delta = p_r - p_t$ . Combining (1) and (2) the Einstein system of equations can be expressed as

$$8\pi\rho = e^{-\lambda} \left[ \frac{\lambda'}{r} - \frac{1}{r^2} \right] + \frac{1}{r^2}, \quad (3)$$

$$8\pi p_r = e^{-\lambda} \left[ \frac{\nu'}{r} + \frac{1}{r^2} \right] - \frac{1}{r^2}, \quad (4)$$

$$8\pi p_t = \frac{e^{-\lambda}}{2} \left[ \nu'' + \frac{\nu'^2}{2} + \frac{\nu'}{r} - \frac{\lambda'}{r} - \frac{\nu'\lambda'}{2} \right], \quad (5)$$

with  $\rho$ ,  $p_r$  and  $p_t$  are the energy density, radial pressure and tangential pressure.

We set  $f(r)$ ,  $g(r)$  and  $h(r)$  as

$$f(r) = e^{-Ar^2} \left[ 2A - \frac{1}{r^2} \right] + \frac{1}{r^2}, \quad (6)$$

$$g(r) = e^{-Ar^2} \left[ 2B + \frac{1}{r^2} \right] - \frac{1}{r^2}, \quad (7)$$

$$h(r) = e^{-Ar^2} \left[ 2B - A + Br^2(B - A) \right]. \quad (8)$$

The system (3)-(5) can be written in reduced form as

$$8\pi\rho = f(r), \quad (9)$$

$$8\pi p_r = g(r), \quad (10)$$

$$8\pi p_t = h(r). \quad (11)$$

The above system can be solved by choosing a particular form of an equation of state. To investigate the effect of dark matter on compact objects we add to the field equations (9)-(11) additional equations of state. We propose a modified general form of the equation state of dark matter calculated using the observational data of the rotational curves of galaxies in Barranco et al. (2015). From our general equation of state, all the known equations of state can

be retrieved. At this point we select an equation of state with the general form

$$p_r = \alpha + \beta\rho + \gamma\rho^n + \eta\sqrt{1 + \theta\rho}. \tag{12}$$

In the above the dimension of the constants  $\alpha, \beta, \gamma, \eta$  and  $\theta$  in CGS unit are  $\alpha$  (dyne  $\text{cm}^{-2}$ ),  $\beta$  (dyne  $\text{g}^{-1} \text{cm}$ ),  $\gamma$  (dyne $^{1/n} \text{g}^{-1/n} \text{cm}^{1/n}$ ),  $\eta$  (dyne  $\text{cm}^{-2}$ ) and  $\theta$  ( $\text{g}^{-1} \text{cm}^3$ ). From the general form we can regain many forms of known equations of state. When  $\gamma = 0$  and  $\eta = 0$  we regain the linear equation of state

$$p_r = \alpha + \beta\rho. \tag{13}$$

When  $n = 2$  and  $\eta = 0$ , then we regain a quadratic equation of state

$$p_r = \alpha + \beta\rho + \gamma\rho^2. \tag{14}$$

When  $\alpha = 0, \beta = 0$  and  $\eta = 0$ , then we regain a polytropic equation of state

$$p_r = \gamma\rho^n. \tag{15}$$

When  $\alpha = 0, n = -\tilde{n}$  and  $\eta = 0$ , then we regain a modified Chaplygin equation of state

$$p_r = \beta\rho + \frac{\gamma}{\rho^{\tilde{n}}}. \tag{16}$$

When  $n = 1/2$  and  $\eta = 0$ , then we regain a color-flavor-locked (CFL) equation of state of Rocha et al. (2019)

$$p_r = \alpha + \beta\rho + \gamma\rho^{1/2}, \tag{17}$$

where  $\alpha = -\left(\frac{\tau}{\pi^2}\right), \beta = \frac{1}{3}$  and  $\gamma = \frac{2\tau}{\pi}$ . When  $\gamma = 0$  and  $\alpha = -\eta$ , then we regain a particular dark matter equation of state from rotational curves (Barranco et al. (2015))

$$p_r = -\eta + \beta\rho + \eta\sqrt{1 + \theta\rho}, \tag{18}$$

where  $\eta = \frac{p_0}{16}, \beta = \frac{3p_0}{4\rho_0}$  and  $\theta = \frac{24}{\rho_0}$ .

### 3 Solutions

#### 3.1 Solution I

The general form of equation (12) is hard to solve analytically but can be solved in reduced form for particular cases. We select the equation of state of dark matter (18) so that

$$p_r = \alpha + \beta\rho + \eta\sqrt{1 + \theta\rho}, \tag{19}$$

where the constant parameters  $\alpha, \beta, \eta$  and  $\theta$  are constrained by the following system

$$p_r(0) = p_r(A, B, \alpha, \beta, \eta, \theta), \tag{20}$$

$$p_t(0) = p_t(A, B, \alpha, \beta, \eta, \theta), \tag{21}$$

$$0 = p_r(B, \mathcal{R}, \alpha, \beta, \eta, \theta). \tag{22}$$

Combining (9)-(10) we get

$$8\pi(\rho + p_r) = f(r) + g(r), \tag{23}$$

which can be solved by specifying an equation of state  $p_r(\rho)$ .

Substituting (19) in (23), we get the solutions for  $\rho$  as

$$\rho = \frac{(1 + \beta)(f + g - 8\pi\alpha) + 4\pi\eta^2\theta}{8\pi(1 + \beta)^2} \pm 2\sqrt{2\pi}\eta[(f + g)(1 + \beta)\theta + 2\pi(4(1 + \beta) \times ((1 + \beta) - \alpha\theta) + \eta^2\theta^2)]^{1/2}/8\pi(1 + \beta)^2. \tag{24}$$

With the new solution (24), the Einstein field equations (9)-(11) can be written as a new exact solution with equation of state from rotational curves of galaxies.

#### 3.2 Solution II

We select the equation of state for CFL matter (17) as

$$p_r = \alpha + \beta\rho + \gamma\sqrt{\rho}, \tag{25}$$

where the constant parameters  $\alpha, \beta$  and  $\gamma$  are constrained by the following system

$$p_r(0) = p_r(A, B, \alpha, \beta, \gamma), \tag{26}$$

$$p_t(0) = p_t(A, B, \alpha, \beta, \gamma), \tag{27}$$

$$0 = p_r(B, \mathcal{R}, \alpha, \beta, \gamma). \tag{28}$$

Combining (9)-(10) we get

$$8\pi(\rho + p_r) = f(r) + g(r), \tag{29}$$

which can be solved by specifying an equation of state  $p_r(\rho)$ . Substituting (17) in (29), we get the solutions for  $\rho$  as

$$\rho = \frac{(1 + \beta)(f + g - 8\pi\alpha) + 4\pi\gamma^2}{8\pi(1 + \beta)^2} \pm 2\sqrt{2\pi}\gamma[(1 + \beta)(f + g - 8\pi\alpha) + 2\pi\gamma^2]^{1/2}/8\pi(1 + \beta)^2. \tag{30}$$

### 4 Physical characteristics of the stellar model

It is important that the physical requirements are satisfied for a realistic star. The physical criteria for the interior of the star

to be well behaved were established in many works including the results of Bondi (1992), Chan et al. (1992), Chan et al. (1993), Herrera and Santos (1997), Mak and Harko (2002) and Mak and Harko (2003).

### 4.1 Regularity requirement within and at surface of the star $r = \mathcal{R}$

The physical requirement for realistic stellar object require that

**A.1.** The potentials  $e^{2\nu}$  and  $e^{2\lambda}$ , the energy density  $\rho$ , radial pressure  $p_r$ , tangential pressure  $p_t$  should be well behaved, positive and not singular within the star;  $\rho$ ,  $p_r$ ,  $p_t$  should be decreasing functions with  $\rho' < 0$ ,  $p_r' < 0$  and  $p_t' < 0$  throughout the stellar structure. We expect the anisotropy to vanish at the centre  $\Delta(r = 0) = 0$  and  $p_t = p_r$ .

**A.2.** The energy conditions within the compact should obey the dominant energy condition (DEC):  $\rho - p_r \geq 0$ , weak energy condition (WEC):  $\rho - p_t \geq 0$  and the strong energy condition (SEC):  $\rho - p_r - 2p_t \geq 0$ . At the boundary  $r = \mathcal{R}$  of the star, the gravitational potentials  $e^{2\lambda}$  and  $e^{2\nu}$  should match to the Schwarzschild exterior metric:

$$e^{\nu(\mathcal{R})} = e^{-\lambda(\mathcal{R})} = 1 - \frac{2M}{\mathcal{R}}. \tag{31}$$

At the boundary  $r = \mathcal{R}$ , the radial pressure  $p_r$  should vanish

$$p_r(\mathcal{R}) = 0. \tag{32}$$

Using the requirements A.1. and A.2., we get different boundary values

$$8\pi\rho(0) = 2A, \tag{33}$$

$$8\pi\rho(\mathcal{R}) = e^{-\mathcal{R}^2 A} \left( 2A - \frac{1}{\mathcal{R}^2} \right) + \frac{1}{\mathcal{R}^2}, \tag{34}$$

$$8\pi p_r(0) = 2B, \quad 8\pi p_t(0) = D, \tag{35}$$

$$8\pi p_t(\mathcal{R}) = e^{-\mathcal{R}^2 A} \left[ D + \mathcal{R}^2 B(D - B) \right], \tag{36}$$

where  $A$ ,  $B$  and the  $D$  (redefined as  $D = 2B - A$ ) are related to the central density, central radial pressure and central tangential pressure.

**A.3.** The stability of the stellar model requires that the speed of sound should be less than the speed of light which leads to  $0 \leq v_r^2 = \frac{dp_r}{d\rho} \leq 1$  and  $0 \leq v_t^2 = \frac{dp_t}{d\rho} \leq 1$  within the stellar structure. The cracking conditions must fulfil  $-1 < v_t^2 - v_r^2 < 0$ ,  $0 < v_r^2 - v_t^2 < 1$ . The adiabatic index should correspond to the following  $\Gamma = \frac{\rho + p_r}{\rho} \frac{d\rho}{dp_r} > \frac{4}{3}$ .

**A.4.** The star’s equilibrium condition represented by the extended Tolman-Oppenheimer-Volkoff (TOV) equation

$$p_r' = -v'(\rho + p_r) + \frac{2}{r}(p_t - p_r). \tag{37}$$

We define

$$F_g = -v'(\rho + p_r), \quad F_h = -\frac{dp_r}{dr},$$

$$F_a = \frac{2}{r}(p_t - p_r),$$

with  $F_g$ ,  $F_h$  and  $F_a$  as gravitational, hydrostatic and anisotropic forces. The equation (37) is written as a sum of all the forces; the sum is expected to be zero for the equilibrium of stellar object

$$F_g + F_h + F_a = 0. \tag{38}$$

**A.5.** The relationship between surface redshift and compactness is given by

$$Z_s(\mathcal{R}) = \frac{1}{\sqrt{1 - \frac{2M(\mathcal{R})}{\mathcal{R}}}} - 1 \tag{39}$$

When the energy conditions in A.2 are met, the two physical quantities  $Z_s$  and  $\mu = \frac{M(\mathcal{R})}{\mathcal{R}}$  should be less than the universal bounds (Ivanov (2017)). In case of the isotropic model the upper bound limits are  $Z_s = 2$  and  $\mu = \frac{M(\mathcal{R})}{\mathcal{R}} = 4/9$  (Buchdahl (1959)). For anisotropic model with positive pressures, when the dominant energy condition (DEC) and the weak energy condition (WEC) are met, then  $Z_s = 5.211$  and  $\mu = \frac{M(\mathcal{R})}{\mathcal{R}} = 0.487$  (Ivanov (2017)). When the strong energy condition (SEC) is met, then  $Z_s = 3.842$  and  $\mu = \frac{M(\mathcal{R})}{\mathcal{R}} = 0.478$  (Ivanov (2002)).

### 4.2 Parameters and constraints

In this section, we describe parameters constrained for acceptability of our model. From (31) the constants  $A$ ,  $B$  and  $C$  are derived by suitable junction conditions imposed at the surface of the star. In terms of the compactness factor  $\mu = \frac{M}{\mathcal{R}}$ , the results are given by

$$A = -\frac{1}{\mathcal{R}} \ln(1 - 2\mu), \tag{40}$$

$$B = \frac{1}{\mathcal{R}^2} \left( \frac{\mu}{1 - 2\mu} \right), \tag{41}$$

$$C = \frac{-\mu}{1 - 2\mu} + \ln(1 - 2\mu). \tag{42}$$

Equations (19), (20) and (22) combined give the following

$$\beta = \frac{p_r(0)}{\rho(0) - \rho(\mathcal{R})} + \frac{H}{\rho(0)\rho(\mathcal{R}) (\rho(0) - \rho(\mathcal{R}))} \tag{43}$$

$$\theta = \frac{1}{\eta^2 \rho(0) \rho(\mathcal{R}) (\rho(0) - \rho(\mathcal{R}))^2} \times [(\alpha^2 - \eta^2) (\rho(0) - \rho(\mathcal{R}))^2 \times (\rho(0) - \rho(\mathcal{R})) - 2\alpha (\rho(0) - \rho(\mathcal{R})) \times (p_r(0) \rho(\mathcal{R}) (\rho(0) + \rho(\mathcal{R})) + H) + p_r(0) \times \rho(\mathcal{R}) (p_r(0) \rho(\mathcal{R}) (\rho(0) + \rho(\mathcal{R})) + H)], \tag{44}$$

where

$$H = [\rho(0) \rho(\mathcal{R}) \times ((\alpha - \eta)(\rho(0) - \rho(\mathcal{R})) - p_r(0) \rho(\mathcal{R})) \times ((\alpha + \eta) \rho(0) - (p_r(0) + \alpha + \eta) \rho(\mathcal{R}))]^{1/2},$$

with following restrictions on parameters  $\alpha$  and  $\eta$

$$\alpha < \frac{p_r(0) \rho(\mathcal{R})}{2(\rho(0) - \rho(\mathcal{R}))}, \tag{45}$$

$$\alpha < \eta < \frac{\rho(\mathcal{R})(p_r(0) + \alpha) - \alpha \rho(0)}{\rho(0) - \rho(\mathcal{R})}. \tag{46}$$

Equations (25), (26) and (28) combined give the following

$$\tilde{\beta} = \frac{\tilde{\alpha} \sqrt{\rho(0)} + \sqrt{\rho(\mathcal{R})} (p_r(0) - \tilde{\alpha})}{\rho(0) \sqrt{\rho(\mathcal{R})} - \rho(\mathcal{R}) \sqrt{\rho(0)}} \tag{47}$$

$$\tilde{\gamma} = \frac{-p_r(0) \rho(\mathcal{R}) + \tilde{\alpha} (-\rho(0) + \rho(\mathcal{R}))}{\rho(0) \sqrt{\rho(\mathcal{R})} - \rho(\mathcal{R}) \sqrt{\rho(0)}}, \tag{48}$$

with the following restriction on the parameter  $\tilde{\alpha}$ :

$$\tilde{\alpha} > \frac{-p_r(0) \rho(\mathcal{R})}{\rho(0) - \rho(\mathcal{R})}, \quad \rho(0) > \rho(\mathcal{R}). \tag{49}$$

### 5 Formulation for compact stars with dark matter components

We presume that the star is composed of two fluids, namely ordinary and dark matter interacting only through gravity, with equations of state  $p_{rN}(\rho_N)$  and  $p_{rD}(\rho_D)$  respectively. The Einstein field equations for hydrostatic equilibrium (i.e. the Tolman Oppenheimer–Volkov (TOV) equations) are written as

$$p_{rN}' = -v'(\rho_N + p_{rN}) + \frac{2}{r}(p_{tN} - p_{rN}), \tag{50}$$

$$p_{rD}' = -v'(\rho_D + p_{rD}) + \frac{2}{r}(p_{tD} - p_{rD}), \tag{51}$$

$$M_N(r) = 4\pi \int r^2 \rho_N dr, \tag{52}$$

$$M_D(r) = 4\pi \int r^2 \rho_D dr, \tag{53}$$

$$M(r) = M_N(r) + M_D(r) \tag{54}$$

$$\delta = \frac{M_D(r)}{M_D(r) + M_N(r)}, \tag{55}$$

where  $M(r) = M_D(r) + M_N(r)$  is the total mass of the dark matter admixed compact star,  $M_D(r)$  is the mass of the dark matter,  $M_N(r)$  the mass of the ordinary matter and  $\delta$  as the mass ratio. The conservation equations of mass for the two fluids (dark matter and ordinary matter) is similar to the equation of each fluids.

Suitable boundary conditions are required to solve the two fluid system.  $M_N$  and  $M_D$  must be equal to zero at the radius  $r = 0$ . From both central densities ( $\rho_D$ ) and ( $\rho_N$ ) given as the initial condition using the equations of state of both fluids, the central radial pressures  $p_{rD}$ ,  $p_{rN}$  are calculated. We solve the two-fluid TOV equations simultaneously, the stellar radius is determined by one of these two radii  $\mathcal{R}_D$  or  $\mathcal{R}_N$ .

We use the equation of state (25) for ordinary matter and (19) for dark matter to compute the system (50)-(55).

### 6 Physical features

We observe that the parameters  $A$ ,  $B$  and  $D$  have the dimension of  $length^{-2}$ . We use the following transformations

$$\tilde{A} = A\mathcal{L}^2, \quad \tilde{B} = B\mathcal{L}^2, \quad \tilde{D} = D\mathcal{L}^2, \tag{56}$$

where  $\mathcal{L}$  is a parameter with dimension of  $length$ . For a particular compactness factor  $\mu$  choose with respect to the equations (40), (42) and (56); the parameters  $\tilde{A}$  and  $\tilde{B}$  can be found. Then from (20) and (22), the central density and pressure are evaluated. With  $\mu = 0.2963$ , equations (43) and (44) lead to the values of  $\beta = -3.961 \times 10^{-17} \text{ dyne g}^{-1} \text{ cm}$  and  $\theta = 111.30 \text{ g}^{-1} \text{ cm}^3$  with free parameters  $\alpha = \frac{-p_r(0)}{26} \text{ dyne cm}^{-2}$ ,  $\eta = p_r(0)/86 \text{ dyne cm}^{-2}$ . Equations (47) and (48) lead to the values of  $\tilde{\beta} = 0.8133 \text{ dyne g}^{-1} \text{ cm}$  and  $\tilde{\gamma} = 0.0417 \text{ dyne}^{1/2} \text{ g}^{-1/2} \text{ cm}^{1/2}$  with free parameters  $\tilde{\alpha} = -p_r(0)/4 \text{ dyne cm}^{-2}$ . These values lead to a particular mass of  $2.01 M_\odot$  with 36.81% contribution of dark matter. By allowing the dark matter central density  $\rho_D(0)$  to vary, we generate different masses, central pressures and radii represented in Table 1, and other physical parameters in Table 2. We find the maximum mass  $2.67 M_\odot$  and radius around 11.16 km with 52.43% as maximum mass limit for an amount of dark matter allowed for the model. The greater value that  $2.01 M_\odot$  can be explained as due to the repulsive interacting strength equilibrium of dark matter particles. Similar statements were made by Xiang et al. (2014), pointing out that the large dark matter fraction in compact stars and the repulsive interactions among dark matter can lead to massive compact stars with mass above  $2.01 M_\odot$ . Other observed pulsars are listed in Table 1, with masses less

than  $2.01 M_{\odot}$ . Our model shows that the admixed dark matter compact star can support a high mass above the known limit of the current observed pulsar PSR J0348+0432 with  $M = 2.01 M_{\odot}$ . It is interesting to point out that change in the value of the mass can be realised by increasing or decreasing the ratio of dark matter. The increase of dark matter in a compact star can provide more gravitational energy with the consequence of compressing the normal matter and leading to a more compact object.

In the case of a star with ordinary matter with mass  $M = 1.30 M_{\odot}$ , with a maximum amount of dark matter mass of  $M = 1.40 M_{\odot}$  corresponding to the Chandrasekhar mass limit as reported in Table 1, the maximum mass of the dark matter admixed compact star does not exceed the mass value of  $M = 2.67 M_{\odot}$ . Furthermore, according to our model, for a given stellar mass, a compact object made of dark matter and ordinary matter is considerably greater than a compact object with only ordinary matter. This feature differs from some previous investigations where it is expected to be otherwise. We noticed a slight decrease in mass of ordinary matter from  $M = 1.30 M_{\odot}$  to  $M = 1.27 M_{\odot}$ , for the maximum mass ratio of  $\delta = 0.5243$ . From Table 2 the compactness factor for the case of a dark matter admixed compact star increases with the increase of dark matter up to the limit allowed by the model. This feature can be justified by the fact that the increase of dark matter could provide more gravitational force leading to more compact object. The presence of dark matter has a non-negligible effect on the mass, radius and other properties of compact stars. The lower mass of ordinary matter  $M = 1.30 M_{\odot}$  slightly decreases by 2.31% for the maximum amount of dark matter  $\delta = 52.81\%$  as shown in Table 1.

To unveil the behaviour of the matter variables within the dark matter admixed star, we have displayed different matter variables in several Figs. 1-4 with 52.40% of dark matter content which leads to the mass of  $M = 2.67 M_{\odot}$  and Figs. 5-14 with 36.80% of dark matter content which leads to the mass of  $M = 2.01 M_{\odot}$ .

### 6.1 Regularity and reality conditions

From our Figs. 1-4 the energy density, radial pressure, tangential pressure and anisotropy profiles are presented for the maximum amount 52.43% of dark matter allowed for our model with maximum mass of  $M_D = 1.40 M_{\odot}$ . The energy density, radial and tangential pressure in Figs. 1, 2, 3, are regular and remains finite. We notice that the dark matter radius, the density, radial pressure, tangential pressure of dark matter are greater than the profiles of ordinary matter. The total density, radial pressure, tangential pressure,  $\rho$ ,  $p_r$  and  $p_t$  are greater than all others profiles of dark matter and ordinary matter. The anisotropy in Fig. 4 is regular at the centre and remains positive inside the stellar structure for the ordinary matter  $\Delta_N$  and the total anisotropy  $\Delta$ . The anisotropic

**Table 1** The amount of the dark matter accreted onto the compact star. The starting stellar mass is fixed to be  $1.30 M_{\odot}$ .  $M_D$ ,  $R_D$ ,  $M_N$ ,  $R_N$ ,  $R$  and  $M = M_N + M_D$  are the respective masses, radii of dark matter, ordinary matter and for dark admixed compact star. The mass ratio  $\delta$  in the first column represents the contribution of dark matter in stellar structure

Star	$\delta$	$p_{rD}(0)$ (dyne $\text{cm}^{-2}$ )	$p_{rN}(0)$ (dyne $\text{cm}^{-2}$ )	$p_r(0)$ (dyne $\text{cm}^{-2}$ )	$M_D$ ( $M_{\odot}$ )	$R_D$ (km)	$M_N$ ( $M_{\odot}$ )	$R_N$ (km)	$M$ ( $M_{\odot}$ )	$R$ (km)
—	0.5243	$1.377 \times 10^{35}$	$1.183 \times 10^{35}$	$2.560 \times 10^{35}$	1.40	12.07	1.27	10.90	2.67	11.16
PSR J0348+0432	0.3681	$1.168 \times 10^{35}$	$1.192 \times 10^{35}$	$2.360 \times 10^{35}$	0.740	7.76	1.27	10.93	2.01	9.95
PSR J1614-2230	0.3551	$1.147 \times 10^{35}$	$1.193 \times 10^{35}$	$2.34 \times 10^{35}$	0.700	7.47	1.28	10.94	1.97	9.86
PSR J1946-3417	0.3001	$1.003 \times 10^{35}$	$1.202 \times 10^{35}$	$2.206 \times 10^{35}$	0.548	5.71	1.28	10.96	1.828	9.31
PSR J2222-0137	0.2771	$9.543 \times 10^{34}$	$1.206 \times 10^{35}$	$2.160 \times 10^{35}$	0.480	5.18	1.28	10.98	1.76	9.18
4U1820-30	0.183	$6.6820 \times 10^{34}$	$1.236 \times 10^{35}$	$1.904 \times 10^{35}$	0.290	2.85	1.29	11.07	1.58	8.86
J2043+1711	0.0650	$1.845 \times 10^{34}$	$1.341 \times 10^{35}$	$1.526 \times 10^{35}$	0.090	0.68	1.29	11.39	1.38	9.10
B1855+09	0	—	$1.341 \times 10^{35}$	—	—	—	1.30	11.39	—	—

**Table 2** Additional physical parameters of the stellar structure with equations of state of ordinary and dark matter

Star	$\tilde{A}_D$	$\rho_D(0)$ (g cm <sup>-3</sup> )	$\rho_N(0)$ (g cm <sup>-3</sup> )	$\rho(0)$ (g cm <sup>-3</sup> )	$\mu = M/\mathcal{R}$	$Z_s$
–	0.200	$1.517 \times 10^{15}$	$2.950 \times 10^{14}$	$1.812 \times 10^{15}$	0.3531	0.8451
PSR J0348+ 0432	0.310	$2.185 \times 10^{15}$	$2.940 \times 10^{14}$	$2.479 \times 10^{15}$	0.2963	0.5670
PSR J1614-2230	0.325	$2.277 \times 10^{15}$	$2.939 \times 10^{14}$	$2.571 \times 10^{15}$	0.2949	0.5614
PSR J1946-3417	0.465	$3.141 \times 10^{15}$	$2.929 \times 10^{14}$	$3.433 \times 10^{15}$	0.2901	0.5420
PSR J2222-0137	0.530	$3.544 \times 10^{15}$	$2.925 \times 10^{14}$	$3.836 \times 10^{15}$	0.2830	0.5179
4U1820-30	1.210	$7.793 \times 10^{15}$	$2.892 \times 10^{14}$	$8.082 \times 10^{15}$	0.2632	0.4531
J2043+1711	6.340	$10.09 \times 10^{15}$	$2.775 \times 10^{14}$	$10.37 \times 10^{15}$	0.2238	0.3455
B1855+09	0	–	$2.775 \times 10^{14}$	–	0.1684	0.2231

profiles for ordinary  $\Delta_N$  and admixed dark matter  $\Delta$  are repulsive, leading to more compact structures (Gokhroo and Mehra (1994)). On the other hand for dark matter  $\Delta_D$ , the anisotropy increases, decreases and becomes negative and then increases as showed in the Fig. 4. To illustrate the behaviour of the matter variables within the dark matter admixed star, we have displayed different matter variables in Figs. 5-14. We used 36.81% of dark matter content which leads to the mass of  $M = 2.01 M_\odot$ .

The maximum mass of dark matter and dark matter admixed compact star allowed by the model is  $M = 1.40 M_\odot$  and  $M = 2.67 M_\odot$ , beyond these values the profiles of matter variables become unphysical and unstable. Moreover, for a given stellar mass, a compact object made of dark matter and ordinary matter is greater than a compact object with only ordinary matter. This feature differs from some previous investigations were it is expected to be otherwise. Also we notice a slight decrease in mass of ordinary matter from  $M = 1.30 M_\odot$  to  $M = 1.27 M_\odot$ , for a maximum mass of dark matter of ratio  $\delta = 0.5243$ . From Table 1, the compactness factor for the dark matter admixed compact star increases with the increase of dark matter in the range of  $\mu = M/\mathcal{R} = 0.2238 - \mu = M/\mathcal{R} = 0.3531$  for the amount dark matter allowed by the model. The similar range of compactness factor were presented by Xiang et al. (2014). Therefore the dark matter amount in compact star can increase to provide more gravitational energy, with the consequence of compressing the normal matter and leading to a more compact object.

### 6.2 Energy and equilibrium conditions

#### 6.2.1 Energy condition

In Fig. 8, the energy conditions  $\rho - p_r$ ,  $\rho - p_t$  and  $\rho - p_r - 2p_t$  are plotted. All the profiles remain positive within the star which shows that the energy conditions are not violated.

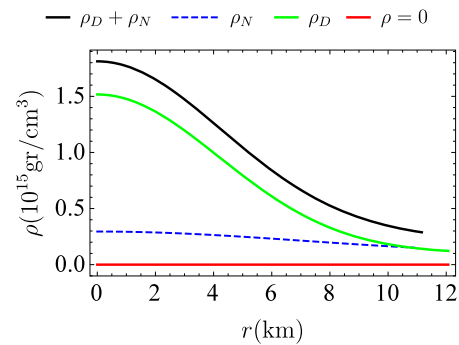


**Fig. 1** Energy density versus radius with 52.43% of dark matter. For  $\rho_D + \rho_N$  (black solid line), for  $\rho_N$  (blue dashed line), for  $\rho = 0$  (red solid line) and for  $\rho_D$  (green solid line)

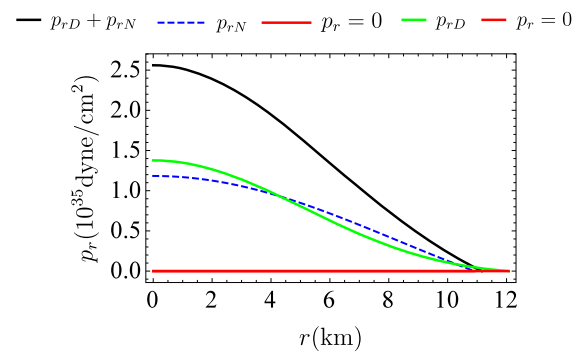


**Fig. 2** Radial pressure versus radius with 52.43% of dark matter. For  $p_{rD} + p_{rN}$  (black solid line), for  $p_{rN}$  (blue dashed line), for  $p_r = 0$  (red solid line) and for  $p_{rD}$  (green solid line)

#### 6.2.2 Equilibrium condition

The features of gravitational ( $F_g$ ), hydrostatic ( $F_h$ ) and anisotropic ( $F_a$ ) forces are displayed in Fig. 9. The two positive forces anisotropic and hydrostatic ( $F_a$  and  $F_h$ ) are balanced by the gravitational force ( $F_g$ ).

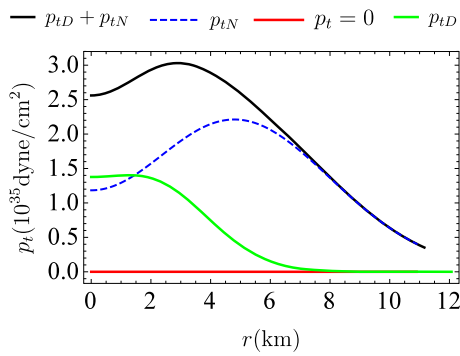


**Fig. 3** Tangential pressure versus radius with 52.43% of dark matter. For  $p_{tD} + p_{tN}$  (black solid line), for  $p_{tN}$  (blue dashed line) and for  $p_r = 0$  (red solid line) and for  $p_{tD}$  (green solid line)

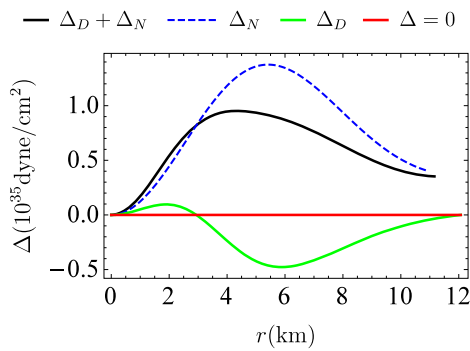


**Fig. 4** Anisotropy versus radius with 52.43% of dark matter. For  $p_r$  (black solid line), for  $p_t$  (blue dashed line) and for  $p_r = p_t = 0$  (red solid line) and  $\Delta$  (green solid line)

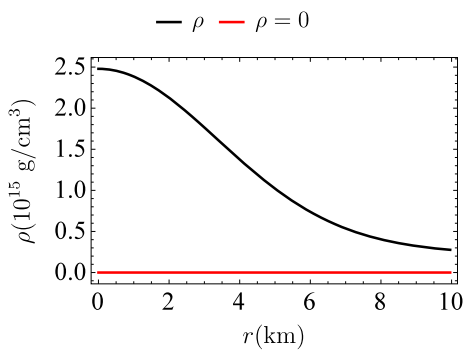


**Fig. 5** Energy density versus radius of PSR J0348+0432 with 36.81% of dark matter. For  $\rho$  (black solid line), for  $\rho = 0$  (red solid line)

### 6.3 Causality conditions and stability

#### 6.3.1 Causality condition

The speed of sound within the star is an essential property to explore. We have plotted in Fig. 10, the radial and tangential speeds of sound  $v_r^2$ ,  $v_t^2$  which comply with the causality condition with respect to the following range  $0 \leq v_r^2 \leq 1$  and  $0 \leq v_t^2 \leq 1$ .

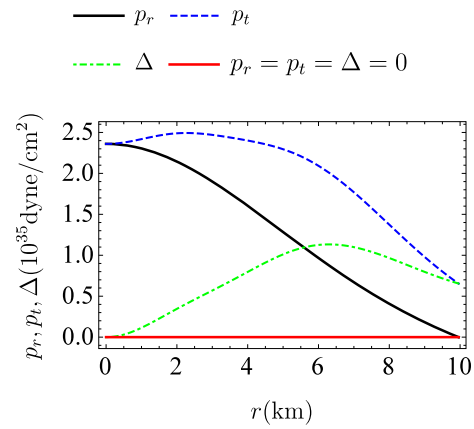


**Fig. 6** Radial pressure, tangential pressure and anisotropy versus radius of PSR J0348+0432 with 36.81% of dark matter. For  $p_r$  (black solid line), for  $p_t$  (blue dashed line), for  $p_r = p_t = 0$  (red solid line) and for  $p_\Delta$  (green dotted dashed)

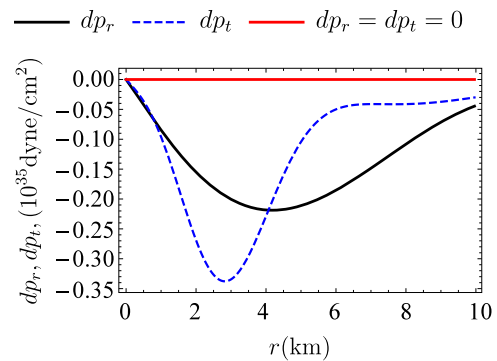


**Fig. 7** Gradient of pressure versus radius of PSR J0348+0432 with 36.81% of dark matter. For  $dp_r$  (black solid line), for  $dp_t$  (blue dashed line) and for  $dp_r = dp_t = 0$  (red solid line)

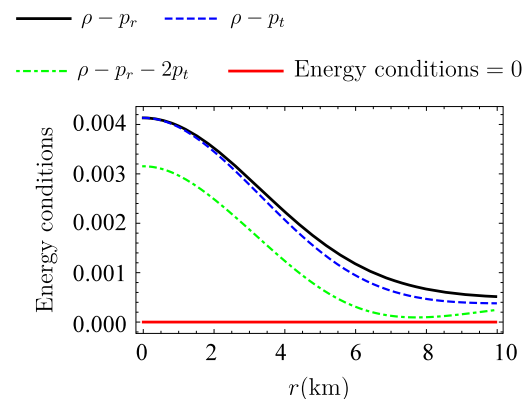


**Fig. 8** Energy conditions versus radius of PSR J0348+0432 with 36.81%. For  $\rho - p_r$  (black solid line), for  $\rho - p_t$  (blue dashed line) and for:  $\rho - p_r - 2p_t$  (Green dotted dashed line)

#### 6.3.2 Stability conditions

To fulfil the Herrera cracking conditions as in Abreu et al. (2007), we show in Fig. 11 the difference of the radial and

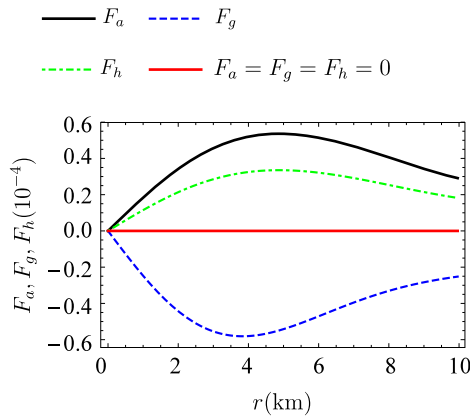


**Fig. 9** Forces  $F_a$ ,  $F_h$  and  $F_g$  versus radius of PSR J0348+0432 with 36.81% of dark matter. For  $F_a$  (black solid line), for  $F_g$  (blue dashed line), for  $F_h$  (green dotted line) and  $F_a + F_g + F_h = 0$  (red solid line)

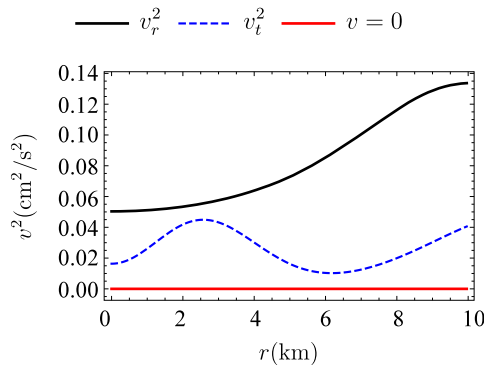


**Fig. 10** Speed of sound versus radius of PSR J0348+0432 with 36.81% of dark matter. For  $v_r^2$  (black solid line), for  $v_t^2$  (blue dashed line) and  $v = 0$  (red solid line)

tangential speeds  $v_r^2 - v_t^2$  and  $v_t^2 - v_r^2$ , where  $v_r^2 - v_t^2$  lies within the interval  $[0,1]$  and  $v_t^2 - v_r^2$  within  $[-1,0]$ . The profiles for the adiabatic indices are presented in Fig. 12. We notice throughout the stellar body that both profiles for the radial and tangential adiabatic indices  $\Gamma_r$  and  $\Gamma_t$  are greater than  $\Gamma = \frac{4}{3}$ .

### 6.4 Redshift and compactness

For anisotropic model with the energy conditions DEC and WEC, the upper bounds are  $Z_s = 5.211$  and  $\mu = \frac{M(\mathcal{R})}{\mathcal{R}} = 0.487$ . With the energy condition SEC, the upper bounds are  $Z_s = 3.842$  and  $\mu = \frac{M(\mathcal{R})}{\mathcal{R}} = 0.478$  (see Ivanov (2002)) and Ivanov (2017)).

To illustrate the above statements, the surface redshift versus the compactness factor is displayed in Fig. 13. The upper bound limit for the maximum compactness factor is  $M/\mathcal{R} = 0.3531$  with a surface redshift limit of  $Z_s = 0.8451$ . The maximum value of the surface redshift and compactness for our model are less than the above mentioned bounds.

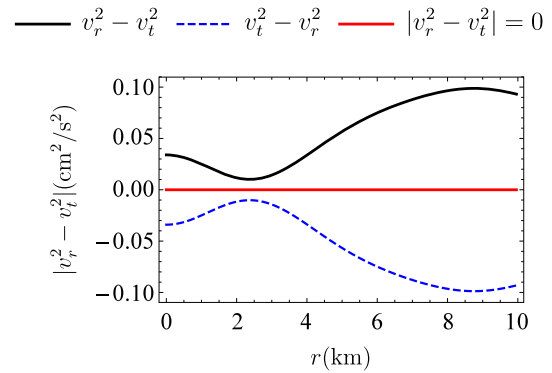


**Fig. 11** The difference of the square radial and tangential speeds of PSR J0348+0432 with 36.81% of dark matter. For  $v_r^2 - v_t^2$  (black solid line) and for  $v_t^2 - v_r^2$  (blue dashed line) and for  $|v_r^2 - v_t^2| = 0$  (red solid line)

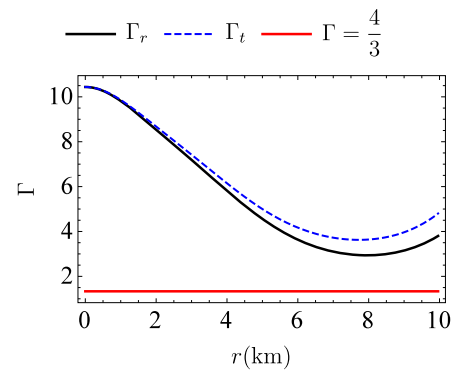


**Fig. 12** Adiabatic index versus radius of PSR J0348+0432 with 36.81% of dark matter. For  $\Gamma_r$  (black solid line) and for  $\Gamma_t$  (blue dashed line) and for  $\Gamma = \frac{4}{3}$  (red solid line)

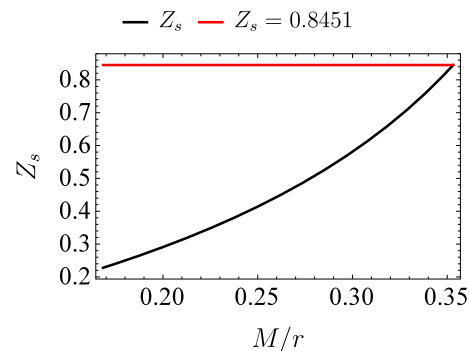


**Fig. 13** The surface redshift versus total mass of compact stars. For  $Z_s$  (black solid line) and for  $Z_s = 0.8451$  (blue dashed line)

The mass against radius for the three cases  $M_D$ ,  $M_N$  and  $M_D + M_D$  is displayed in the Fig. 13. It shows the mass of the compact star as a function of radius for 36.81% of dark matter content. For comparison, we present in the same figure the mass versus radius for three cases: dark matter (lower curve in green dashed), ordinary matter (middle curve in blue dashed) and dark matter admixed compact star (upper

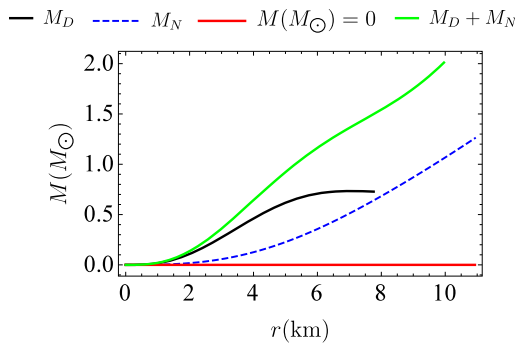


**Fig. 14** Mass versus radius. For the dark matter  $M_D$  (black solid line) with  $M = 0.73 M_\odot$ . For the ordinary matter  $M_N$  (blue dashed line) with  $M = 1.27 M_\odot$ . For the dark matter admixed compact stars  $M_D + M_N$  (green solid line) with  $M = 2.01 M_\odot$

curve in black solid). We notice a lower mass for dark matter compared to the mass of ordinary matter. Both profiles have lower masses compared to the mass of the dark matter admixed compact star.

## 7 Conclusion

In this paper we have studied exact models using an equation of state for dark matter and ordinary matter to model compact stars. The assumption used is that dark matter and ordinary matter interact only through gravity. We have found different masses of known observed stars in the range from  $1.38 M_\odot$  to  $2.67 M_\odot$  for a dark matter admixed compact star with different ratio of dark matter contribution. The results show that the star compactness factor can be influenced by the presence of a certain amount of dark matter within the star. Our observation is that the presence of dark matter in compact stars can increase the compactness factor in the presence of an equation of state relevant for the rotational curves of galaxies. The compactness factor and surface redshift values are in agreement with required conditions. From this study, we can conclude that the equation of state from the rotational curves of galaxies can be used in the exact solution approach in modelling dark matter admixed compact stars. It is interesting to observe that another exact approach in studying stellar objects is embedding where the 4-dimensional curved manifold is embedded in a flat 5-dimensional Euclidean space. This approach is also relevant in the modelling of dark matter in the rotational curves galaxies with color-flavor-locked CFL distributions. As demonstrated in Singh et al. (2020a), Govender et al. (2020) and Singh et al. (2020b) the embedding approach also produces physically acceptable results with relevant equations of state.

**Acknowledgements** PMT and LLL thank the University of South Africa and National Research Foundation for financial support. SDM

acknowledges that this work is based on research supported by the South African Research Chair Initiative of the Department of Science and Technology and the National Research Foundation.

**Publisher's Note** Springer Nature remains neutral with regard to jurisdictional claims in published maps and institutional affiliations.

## References

- Abreu, H., Hernandez, H., Nunez, L.A.: *Class. Quantum Gravity* **24**, 4631 (2007)
- Ade, P.A.R., et al.: *Astron. Astrophys.* **594**, A13 (2016)
- Alcock, C., Farhi, E., Olinto, A.: *Astrophys. J.* **310**, 261 (1986)
- Alford, M., Braby, M., Paris, M.W., Reddy, S.: *Astrophys. J.* **629**, 969 (2005)
- Angeles, M., Garca, P., Silk, J.: *Phys. Lett. B* **711**, 6 (2012)
- Arcadi, G., Catena, R., Ullio, P.: (2012). [arXiv:1211.5129](https://arxiv.org/abs/1211.5129) [hep-ph]
- Barranco, J., Bernal, A., Nunez, D.: *Mon. Not. R. Astron. Soc.* **449**, 403 (2015)
- Benvenuto, O.G., Horvath, J.E.: *Mon. Not. R. Astron. Soc.* **241**, 43 (1989)
- Bodmer, A.R.: *Phys. Rev. D* **4**, 1601 (1971)
- Bondi, H.: *Mon. Not. R. Astron. Soc.* **259**, 395 (1992)
- Buchdahl, H.A.: *Phys. Rev.* **116**, 1027 (1959)
- Chan, R., Herrera, L., Santos, N.O.: *Class. Quantum Gravity* **9**, 133 (1992)
- Chan, R., Herrera, L., Santos, N.O.: *Mon. Not. R. Astron. Soc.* **265**, 533 (1993)
- Chodos, A., Jaffe, R.L., Johnson, K., Thorne, C.B., Weisskopf, V.F.: *Phys. Rev. D* **9**, 3471 (1974)
- Ciarcellut, P., Sandin, F.: *Phys. Lett. B* **695**, 19 (2011)
- Farhi, E., Jaffe, R.L.: *Phys. Rev. D* **30**, 2379 (1984)
- Feng, J.L.: (2012). [arXiv:1211.3116](https://arxiv.org/abs/1211.3116) [astro-ph.HE]
- Gokhroo, M.K., Mehra, A.L.: *Gen. Relativ. Gravit.* **26**, 5 (1994)
- Govender, M., Maharaj, A., Singh, K.N., Pant, N.: *Mod. Phys. Lett. A* **35**, 2050164 (2020)
- Haensel, P., Zdunik, J.L., Schaeffer, R.: *Astron. Astrophys.* **160**, 21 (1986)
- Herrera, L., Santos, N.O.: *Phys. Rep.* **286**, 53 (1997)
- Itoh, N.: *Prog. Theor. Phys.* **44**, 291 (1970)
- Ivanov, B.V.: *Phys. Rev. D* **65**, 104011 (2002)
- Ivanov, B.V.: *Eur. Phys. J. C* **77**, 738 (2017)
- Ivanenko, D.D., Kurdgelaidze, D.F.: *Astrophysics* **1**, 251 (1965)
- Kouvaris, C., Tinyakov, P.: *Phys. Rev. D* **82**, 063531 (2010)
- Krori, K.D., Barua, J.: *J. Phys. A, Math. Gen.* **8**, 508 (1975)
- Leung, S.C., Chu, M.C., Lin, L.M.: *Phys. Rev. D* **84**, 107301 (2011)
- Li, A., Huang, F., Xu, R.X.: *Astropart. Phys.* **37**, 70 (2012)
- Lugones, G., Horvath, J.E.: *Phys. Rev. D* **66**, 074017 (2002)
- Lugones, G., Horvath, J.E.: *Astron. Astrophys.* **403**, 173 (2003)
- Mak, M., Harko, T.: *Chin. J. Astron. Astrophys.* **2**, 248 (2002)
- Mak, M., Harko, T.: *Proc. R. Soc. Lond. A* **459**, 393 (2003)
- Mukhopadhyay, P., Schaffner-Bielich, J.: *Phys. Rev. D* **93**, 083009 (2016)
- Rahaman, F., Sharma, R., Ray, S., Maulick, R., Karar, I.: *Eur. Phys. J. C* **72**, 2071 (2012)
- Rezaei, Z.: *Astrophys. J.* **835**, 33 (2017)
- Rezaei, Z.: *Int. J. Mod. Phys. D* **27**, 1950002 (2018)
- Rocha, L.S., Bernardo, A., de Avellar, M.G.B., Horvath, J.E.: *Astron. Notes* **340**, 180 (2019)
- Sandin, F., Ciarcelluti, P.: *Astropart. Phys.* **32**, 278 (2009)
- Sharif, M., Saba, S.: *Eur. Phys. J. C* **78**, 921 (2018)
- Singh, K.N., Maurya, S.K., Errehymy, A., Rahaman, F., Daoud, M.: *Phys. Dark Universe* **30**, 100620 (2020a)

- Singh, K.N., Bisht, R.K., Maurya, S.K., Pant, N.: *Chin. Phys. C* **44**, 035101 (2020b)
- Terazawa, H., Akama, K., Chikashige, Y.: *Prog. Theor. Phys.* **60**, 1521 (1978)
- Weber, F.: *Prog. Part. Nucl. Phys.* **54**, 193 (2005)
- Witten, E.: *Phys. Rev. D* **30**, 272 (1984)
- Xiang, Q.F., Jiang, W.Z., Zhang, D.R., Yang, R.Y.: *Phys. Rev. C* **89**, 025803 (2014)